

# Measurements and Performance Factor Comparisons of Magnetic Materials at High Frequency

Alex J. Hanson, *Student Member, IEEE*, Julia A. Belk, *Student Member, IEEE*, Seungbum Lim, *Student Member, IEEE*, Charles R. Sullivan, *Fellow, IEEE*, and David J. Perreault, *Fellow, IEEE*

**Abstract**—The design of power magnetic components for operation at high frequency (HF, 3–30 MHz) has been hindered by a lack of magnetic material performance data and by the limited design theory in that frequency range. To address these deficiencies, we have measured and present core loss data for a variety of commercially available magnetic materials in the HF range. In addition, we extend the theory of performance factor for appropriate use in HF design. Since magnetic materials suitable for HF applications tend to have low permeability, we also consider the impact of low permeability on design. We conclude that, with appropriate material selection and design, increased frequencies can continue to yield improved power density well into the HF regime.

**Index Terms**—High frequency, very high frequency, power conversion, magnetics, ferrites, core loss, Steinmetz parameters

## I. INTRODUCTION

MAGNETIC components (e.g. inductors and transformers) are typically the largest and most lossy components in power converters [1]. While increasing converter switching frequencies can reduce the required size of passive components, size reductions achievable through frequency increases are often limited by core loss (such as in transformers and resonant inductors) [2]; moving beyond operating frequency limits dictated by core loss characteristics can result in unacceptable efficiencies. These concerns have been a significant part of focused research to integrate power supplies “on-chip” (PwrSoC) and “in-package” (PwrSiP) [3]–[5] at low power levels, and towards increased miniaturization and integration at higher power levels. In spite of the challenges, recent research has made significant advances in miniaturized power converters operating in the high frequency (HF) and very high frequency (VHF) ranges<sup>1</sup> (3–300 MHz) (e.g. [6]–[15]), well above typical modern designs operating from hundreds of kilohertz to a few megahertz.

A.J. Hanson, J.A. Belk, S. Lim, and D.J. Perreault are with the Electrical Engineering and Computer Science Department at the Massachusetts Institute of Technology, Cambridge, MA 02139 USA (e-mail: ajhanson@mit.edu, jabelk@mit.edu, sblim@mit.edu, djperrea@mit.edu).

C.R. Sullivan is with the Thayer School of Engineering at Dartmouth College, Hanover, NH 03755 USA (e-mail: charles.r.sullivan@dartmouth.edu).

<sup>1</sup>We follow the International Telecommunication Union (ITU) definitions of frequency ranges, e.g. “Low Frequency” (LF) (30–300 kHz), “Medium Frequency” (MF) (300 kHz–3 MHz), “High Frequency” (HF) (3–30 MHz), and “Very High Frequency” (VHF) (30–300 MHz). The term “Radio Frequency” (RF) is used here (as is commonly done) to refer to those bands most used for wireless communication, i.e. the HF range and above. We continue to use the term “high frequency” (without the acronym HF) to refer to frequencies that are relatively high for power conversion applications, but may not fall specifically in the HF range.

While advances in high-frequency power electronics have been substantial, the design of power magnetics is still not fully understood or optimized, especially in the HF range where use of low-permeability radio frequency (RF) magnetic materials can play a valuable role. In part, this owes to a lack of data regarding HF magnetic materials. Magnetic materials intended for power conversion are typically characterized for core loss under high flux drive, either by empirically determined graphs relating ac magnetic field amplitude, frequency, and volumetric power loss, or through equivalent representations such as Steinmetz parameters. However, large-signal loss data are simply not available for most magnetic materials above a few megahertz, hindering detailed design of power magnetics at these frequencies. Additionally, the modeling and evaluation methods for magnetic components must be adapted in the HF range. Great efforts have been made to model magnetic core loss and winding loss, but holistic design and evaluation remain incomplete.

To address these deficiencies, we present analysis and experimental data for HF magnetic component design. We present a modified performance factor metric to evaluate magnetic materials at HF, experimental measurements of core loss in magnetic materials suitable for HF operation, and a discussion of the effects of low permeability (common to HF materials) on component design. This paper expands on the work previously published in the related conference paper [16], including data for 6 additional materials and a thorough extension to the performance factor metric to include permeability.

In Section II, we discuss the features and limits of the magnetic material *performance factor*,  $\mathcal{F} = \hat{B}f$ . As traditionally defined, the performance factor assumes that winding loss is independent of frequency, which is often not true in the HF range. We therefore introduce and discuss a *modified performance factor*,  $\mathcal{F}_w = \hat{B}f^w$ , which is intended to take into account the effects of high-frequency winding loss in the design of magnetic components. The winding parameter  $w$  takes on values between  $\frac{1}{2}$  and 1 depending on winding design constraints; the choice of  $w = 1$  neglects ac effects on winding resistance and returns the traditional performance factor  $\mathcal{F}$ .

In Section III (and Appendix A), we present core loss data gathered using the method developed in [17] and outlined in Appendix B. These results are meant to fill the aforementioned gap in available loss data and facilitate better magnetics design in the HF range. Results are presented for 20 commercially available materials (mostly NiZn ferrites) for which loss data have not been previously available, primarily in the 2–20 MHz

range. The materials span a variety of manufacturers and permeabilities and represent a large proportion of materials available in this space.

In Section IV, the measured data, in conjunction with the limited previous data available from manufacturers and in the literature, are applied to the discussion of performance factor and the modified performance factor presented in Section II, in order to provide some insights into the design of power electronics in the HF range. We further utilize the results from Section III to show the practical impact on the size and quality factor of HF inductors.

In Section V we address the impact of low permeabilities ( $\mu_r$  from about 4 to 400) on the design of magnetic components, since low permeabilities are common for HF magnetic materials (due to fundamental physical tradeoffs between permeability and core loss). We introduce the principle of diminishing returns on permeability and conclude that modest permeabilities can be sufficient for effective magnetic component design at HF.

Section VI presents our general conclusions. In particular, we foresee significant power density improvements for power magnetics operating well into the HF range.

## II. PERFORMANCE FACTORS

A popular way to evaluate the capability of magnetic materials for power conversion applications across a range of frequencies is the “performance factor” [18]–[27]

$$\mathcal{F} = \hat{B} \cdot f \quad (1)$$

where  $f$  is the frequency of operation under consideration and  $\hat{B}$  is the peak amplitude of ac flux density that results in a specified power loss per unit volume  $P_v$ , taken to be the maximum practical allowable power dissipation per unit volume. Typical values of  $P_v$  are 200 mW/cm<sup>3</sup> (a conservative value), 300 mW/cm<sup>3</sup> (a moderate value), or 500 mW/cm<sup>3</sup> (for small volumes, planar geometries, and/or active cooling). Performance factor is designed to be proportional to the power or VA handling possible with a given core, and is relevant as a design metric for applications such as transformers and resonant inductors where core loss is a major design constraint.

Performance factor is developed considering limitations on power loss for a given core size, under several assumptions. The first assumption is to neglect variations in ac winding resistance (and hence winding loss) with frequency such that, for a given winding, the achievable ampere-turns ( $NI_{max}$ ) is independent of the frequency. The second assumption is that the waveform shapes are sinusoidal, and the third assumption is that the flux density is limited by power loss in the core, not by saturation. Because the instantaneous voltage across a winding is proportional to  $dB/dt$ , the maximum rms value of the voltage at a given power loss per volume  $P_v$  is proportional to magnetic flux density and frequency,  $V_{max} \propto \hat{B} \cdot f$ . Given fixed waveform shapes, the power or VA is proportional to the product of rms current and voltage, and thus to the performance factor.

$$VA = V_{max} I_{max} \propto (\hat{B}f) \times (I_{max} = \text{constant}) \propto \mathcal{F} \quad (2)$$

A plot of performance factor as a function of frequency for a collection of materials provides a quick way to compare materials and identify the highest performance materials at a given frequency, or to identify the frequency range where a particular material is most useful [28]. However, the assumptions underlying the traditional performance factor impose some limits on its usefulness, and some modified performance factors have been proposed to overcome these limits. In [29], a modified performance factor is proposed to consider saturation flux density also. The proposal is to simply take the geometric mean of saturation flux density (a consideration for dc current) and conventional performance factor (a consideration for ac current) to obtain  $\mathcal{F}_{dc+ac} = \sqrt{B_s \cdot \mathcal{F}}$ . Although no rigorous justification is given for this formulation, it appears to be useful in design examples provided in [29]. In [30], another modified performance factor is proposed,  $\mathcal{F}_{\frac{3}{4}} = \hat{B}f^{\frac{3}{4}}$ . The  $\frac{3}{4}$  exponent is said to account for high-frequency winding effects.

At MHz frequencies, high-frequency winding effects are consistently important, and magnetics design is often dominated by core loss rather than saturation considerations. Thus, we choose to examine  $\mathcal{F}_{\frac{3}{4}}$  in more detail. First we note that for comparing different materials at a fixed frequency, the choice between conventional ( $\mathcal{F}$ ) and modified ( $\mathcal{F}_{\frac{3}{4}}$ ) performance factors does not matter—either will lead to the same conclusions as they differ by only a fixed factor of  $f^{\frac{1}{4}}$ . However, if the goal is to select an operating frequency, they may lead to different conclusions, with  $\mathcal{F}$  indicating a larger benefit to increasing frequency, but with that advantage discounted based on high-frequency winding loss when  $\mathcal{F}_{\frac{3}{4}}$  is used.

We extend the theory in [30] and designate  $\mathcal{F}_w = \hat{B}f^w$  as the modified performance factor, where  $w$  is a parameter selected based on the analysis of winding loss in each case. The choice of  $f^{\frac{3}{4}}$  in [30] is based on the assumption that  $R_{ac} \propto f^{\frac{1}{2}}$ , as is the case with simple skin effect. To maintain a constant power loss in a given winding, the maximum current handling is proportional to  $1/\sqrt{R_{ac}}$ , which is proportional to  $f^{-\frac{1}{4}}$ . More generally, for fixed loss with varying numbers of turns,  $I \propto f^{-\frac{1}{4}}/N$ . The voltage is proportional to  $N\hat{B}f$ , so the product of voltage and current is proportional to  $\hat{B}f^{\frac{3}{4}}$ . Hence  $\mathcal{F}_{\frac{3}{4}}$  is appropriate for components with windings whose ac resistance is determined by simple skin effect, and thus is a good choice for use in the HF range.

However, in many practical situations the assumption that winding resistance is dominated by skin effect is not valid. In particular, for multi-layer windings including litz wire windings, proximity effect is also important. To determine the appropriate type of modified performance factor to use for these cases, we assume that the winding is optimized for the particular frequency to be used. As discussed in [31], there are several possible constraints one might adopt for optimizing a multi-layer winding, so we consider each in turn to find the corresponding modified performance factor,  $\mathcal{F}_w = \hat{B}f^w$ . The results, derived below, are listed in Table I.

One scenario is a multi-layer winding with a fixed number of layers, with the conductor thickness in each layer optimized to minimize ac resistance at the operating frequency. This is Case 2 in [31] and is also the case considered in the winding

optimization analysis in [32]. The result, for  $p$  layers, is an optimized winding resistance that is reduced by a factor of  $1/\sqrt{p}$  from the resistance of a single-layer winding, using a layer thickness of approximately  $1.3\delta/\sqrt{p}$ . Thus, the frequency dependence is the same as for a single-layer winding, which is simply the case in which the fixed value of  $p$  is equal to 1, and for any fixed value of  $p$ , the appropriate modified performance factor is  $\mathcal{F}_{\frac{3}{4}} = \hat{B}f^{\frac{3}{4}}$ .

Unfortunately, for frequencies in the HF range, the optimum thickness for a many-layered winding can be thinner than is easily practical. Litz wire becomes very expensive with strands smaller than  $50\mu\text{m}$  in diameter and is not commercially available with strands smaller than about  $30\mu\text{m}$ . Although foil is available at low cost down to single-digit micrometer thicknesses, applying it effectively in multiple parallel layers can be difficult [33]. Thus, another situation of interest is a minimum thickness constraint on the layers of a multi-layer winding. In this case, as reviewed in [31], the resistance is reduced relative to the resistance of a single-layer winding by a factor of about  $\frac{2}{3} \frac{t_{min}}{\delta}$ , where  $t_{min}$  is the minimum thickness constraint and  $\delta$  is the skin depth, for thicknesses below about 1.5 skin depths. Given that the resistance of a single-layer winding is proportional to  $1/\delta$ , we see the optimized multi-layer design under this constraint has resistance proportional to  $1/\delta^2$ , and thus proportional to frequency. As shown in Table I, this results in a modified performance factor  $\mathcal{F}_{\frac{1}{2}} = \hat{B}f^{\frac{1}{2}}$ . It is important to note this is only valid for combinations of frequency and minimum thickness such that  $t_{min} < 1.5\delta$ ; beyond that point, a single layer would be preferable, and  $\mathcal{F}_{\frac{3}{4}}$  should be used instead.

A particular example of this is litz wire for which we take AWG 48 ( $32\mu\text{m}$ ) as the smallest practical strand diameter,  $d_{min}$ . The corresponding effective layer thickness is  $0.584d_{min}$  [31], or  $18.7\mu\text{m}$ . This is equal to  $1.5\delta$  at 28 MHz at room temperature in copper, indicating in this case that magnetic materials could be evaluated using  $\mathcal{F}_{\frac{1}{2}}$  for frequencies up to 28 MHz. The lower power of  $f$  ( $\frac{1}{2}$  instead of  $\frac{3}{4}$ ) in the performance factor for this case indicates the diminishing value of litz wire over the HF frequency range, and in practice, litz wire is not usually worthwhile above the low end of the HF range (though it has been used effectively in the 5–10 MHz range, e.g. [15], [34]).

A third case is a multi-layer winding with a fixed number of wire strands, with the strand diameter optimized. With the number of strands  $n$  fixed at one, this corresponds to a simple solid-wire winding. Larger values of  $n$  correspond to litz wire with a fixed number of strands. As the diameter of the strands is varied, the number of turns that fit in one layer of the winding varies, and so the number of layers varies. Thus, this case is different from the case of a fixed number of layers. Designs optimized under this constraint have a ratio of ac resistance to dc resistance  $F_r = 1.5$ , and wire diameter proportional to  $1/f^{\frac{1}{3}}$  [35], [36]. This results in ac resistance proportional to  $f^{\frac{2}{3}}$ , and  $\mathcal{F}_{\frac{2}{3}} = \hat{B}f^{\frac{2}{3}}$ . In the HF range, multi-layer solid-wire windings are a poor choice and litz wire is limited by strand diameter rather than by the feasible or economical number of strands. Thus, this version of modified performance factor is more relevant to the LF than to the HF

TABLE I: Optimized ac resistance as a function of frequency for different assumptions and resulting performance factor formulation

Case	$R_{ac}$ vs. $f$	$NI$ vs. $f$	Corresponding performance factor
No significant ac resistance effects	$R_{ac} \propto f^0$	$NI \propto f^0$	$\mathcal{F}_1 = \hat{B}f$
Single-layer winding or other fixed number of foil layers or effective wire layers	$R_{ac} \propto f^{\frac{1}{2}}$	$NI \propto f^{-\frac{1}{4}}$	$\mathcal{F}_{\frac{3}{4}} = \hat{B}f^{\frac{3}{4}}$
Fixed layer or strand thickness	$R_{ac} \propto f$	$NI \propto f^{-\frac{1}{2}}$	$\mathcal{F}_{\frac{1}{2}} = \hat{B}f^{\frac{1}{2}}$
Fixed number of wire strands with many layers	$R_{ac} \propto f^{\frac{2}{3}}$	$NI \propto f^{-\frac{1}{3}}$	$\mathcal{F}_{\frac{2}{3}} = \hat{B}f^{\frac{2}{3}}$

range, but it is included in Table I for completeness.

A final case to consider is one in which an advanced winding technology eliminates skin- and proximity-effect losses and makes the ac resistance equal to the dc resistance, and the achievable winding resistances is not limited by number of strands, number of layers, or a minimum thickness constraint, but instead by the available space in the winding window. In this case, the ordinary performance factor  $\mathcal{F}$  is the appropriate measure, just as it is for lower frequency designs where skin and proximity effects are not significant. For example, at tens of kilohertz, litz wire can perform well enough in many cases that an initial design can be based on the assumption that skin and proximity effect are eliminated, although care is needed in the litz wire design to ensure that this goal is achieved [37]. For HF windings, skin and proximity effect are still serious issues even with the best available litz wire. Possible methods to make HF windings that approach the performance of litz wire at lower frequencies are discussed in [33].

The different performance factors in Table I can be summarized as follows:

- Without significant ac resistance effects, conventional performance factor is appropriate.
- With ac resistance effects, and with a single-layer winding, as is often the most practical solution for frequencies in the HF range, the appropriate modified performance factor is  $\mathcal{F}_{\frac{3}{4}}$ . This result also applies to any fixed number of layers, if the thickness of the layers is optimized for the frequency of operation.
- If the fixed constraint is instead the minimum layer thickness or wire diameter, and the number of layers or strands is optimized for the frequency of operation, the appropriate performance factor is  $\mathcal{F}_{\frac{1}{2}}$ .
- The intermediate case of a multilayer wire winding with a fixed number of strands results in  $\mathcal{F}_{\frac{2}{3}}$ , but is rarely relevant to the HF range.

Thus, in our generalized definition of high-frequency performance factor  $\mathcal{F}_w = \hat{B}f^w$ , we choose values of  $w$  between  $\frac{1}{2}$  and 1 based on the winding design constraints anticipated in the application of interest. Because a single-layer winding is the most common choice for frequencies in the HF range, we choose to use  $w = \frac{3}{4}$ , and thus  $\mathcal{F}_{\frac{3}{4}} = \hat{B}f^{\frac{3}{4}}$  for comparing core materials in Section IV (in addition to traditional per-

formance factor  $\mathcal{F} = \hat{B}f$ ). Nevertheless, for specific types of winding designs and different frequency ranges, the different modified performance factors listed in Table I can be chosen accordingly.

### III. MEASURED CORE LOSS DATA

In order to use the performance factor in its original or modified form it is necessary to have core loss data for a variety of materials across the frequency range of interest. As discussed in the introduction, there is a significant lack of core loss data available in the HF range for several reasons. First, it is very difficult to accurately measure core loss at frequencies above a few MHz accurately; doing so requires novel techniques that are incompatible with traditional methods used by automated core loss measurement equipment [17]. Additionally, there are few economic incentives to publish core loss data at HF. The automated equipment that manufacturers use to measure core loss at LF (which is inaccurate at HF) is already prohibitively expensive, and few of the traditional markets for HF materials consider large signal core loss an important parameter. Manufacturers of these materials often include graphs of complex permeability from which the small-signal loss tangent  $\tan \delta = \mu''/\mu'$  can be calculated; unfortunately the loss tangent calculated from this data cannot be extrapolated to predict large-signal characteristics required for power electronics applications. Nevertheless, some initial data at the edge of the HF range are available: datasheets include core loss data for materials up to a few megahertz [28], and the literature contains some sparse data in the VHF (30–300 MHz) range [17]. Core loss data within the HF range are necessary for design in general and to apply theoretical extensions like those in Section II.

Using the method described in Appendix B, we have measured core loss characteristics for materials of various types and permeabilities from several manufacturers. Data were primarily gathered in the range of 2–20 MHz, as this represents the greatest dearth in available data. Core loss data with fitted curves can be shown graphically as in Fig. 1.

Core loss data can also be represented algebraically by the Steinmetz equation,  $P_v = k\hat{B}^\beta$ , where  $k$  and  $\beta$  are known as the Steinmetz parameters [38]. Parameters for materials are empirically determined by curve fitting from the same experimental data used to create loss charts like those in Fig. 1. In this formulation of the Steinmetz equation, independent values of  $k$  and  $\beta$  are required for each frequency. Values of  $k$  and  $\beta$  for all measured materials at all measured frequencies are listed in Table II, including 14 materials reported in [16] and 6 additional materials.

It is well known that dc bias can have significant impact on core loss [44], [45]. This is certainly true for low-permeability RF magnetic materials (including NiZn ferrites), as we illustrate in Appendix C. It is also known, for some ferrites, that the combination of high permittivity and high permeability in very large cores can lead to dimensional resonance and flux skin effect phenomena at high frequencies [46], [47]. These effects can cause changes in permeability and increased losses at higher frequencies and in larger core sizes. While these

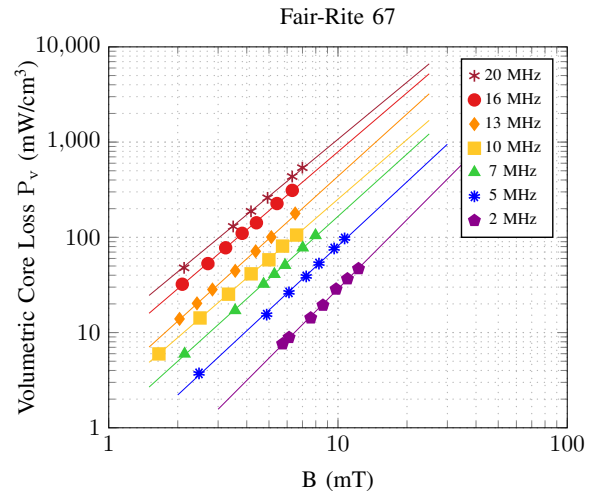


Fig. 1: Core loss data from Fair-Rite 67 as a sample material suitable for HF operation. Fair-Rite 67 has a nominal relative permeability  $\mu_r = 40$ .

effects can be significant in large cores, they are unlikely to be significant in the small cores ( $\sim 1$  cm) of low permeability ( $\mu_r \sim 100$ ) studied here. These effects were not directly observed in the experiments outlined here, and will not be considered further in this paper.

### IV. EXPERIMENTAL PERFORMANCE FACTOR ANALYSIS AND COMPARISON

Performance factor  $\mathcal{F}$  and modified performance factor  $\mathcal{F}_{\frac{3}{4}}$  were calculated using the core loss data represented by the parameters in Table II. The magnetic flux densities corresponding to a loss density of  $P_v = 500$  mW/cm<sup>3</sup> were found and used to compute the performance factor  $\mathcal{F} = \hat{B}f$  and modified performance factor  $\mathcal{F}_{\frac{3}{4}} = \hat{B}f^{\frac{3}{4}}$ . The standard and modified performance factors are plotted in Figures 2 and 3 respectively. (In this section, we focus on  $\mathcal{F}_1$  and  $\mathcal{F}_{\frac{3}{4}}$  due to their applicability in typical HF designs, as discussed in Section II. The other performance factors appropriate to different winding configurations are plotted in Appendix A).

Performance factor data are also included from Ferroxcube [28], with modified performance factor calculated from the listed data as  $\mathcal{F}_{\frac{3}{4}} = \mathcal{F}/f^{\frac{1}{4}}$ . These data come from MnZn ferrites optimized for different frequency ranges, and one NiZn ferrite material (4F1), and are representative of available materials at low frequency. Each point on the Ferroxcube curve represents the highest performance factor among Ferroxcube materials at a particular frequency. Both standard and modified performance factors are also calculated for the VHF data presented in [17].

Fig. 2 shows that the maximum performance factor of available materials increases roughly as the square root of frequency between 20 kHz and 100 kHz, providing a good opportunity for improved power density through increasing frequency in that range. Between 100 kHz and 2 MHz, the improvement rate is slower, and is on average approximately proportional to  $f^{\frac{1}{4}}$ . This indicates that, although increasing

### Standard Performance Factor

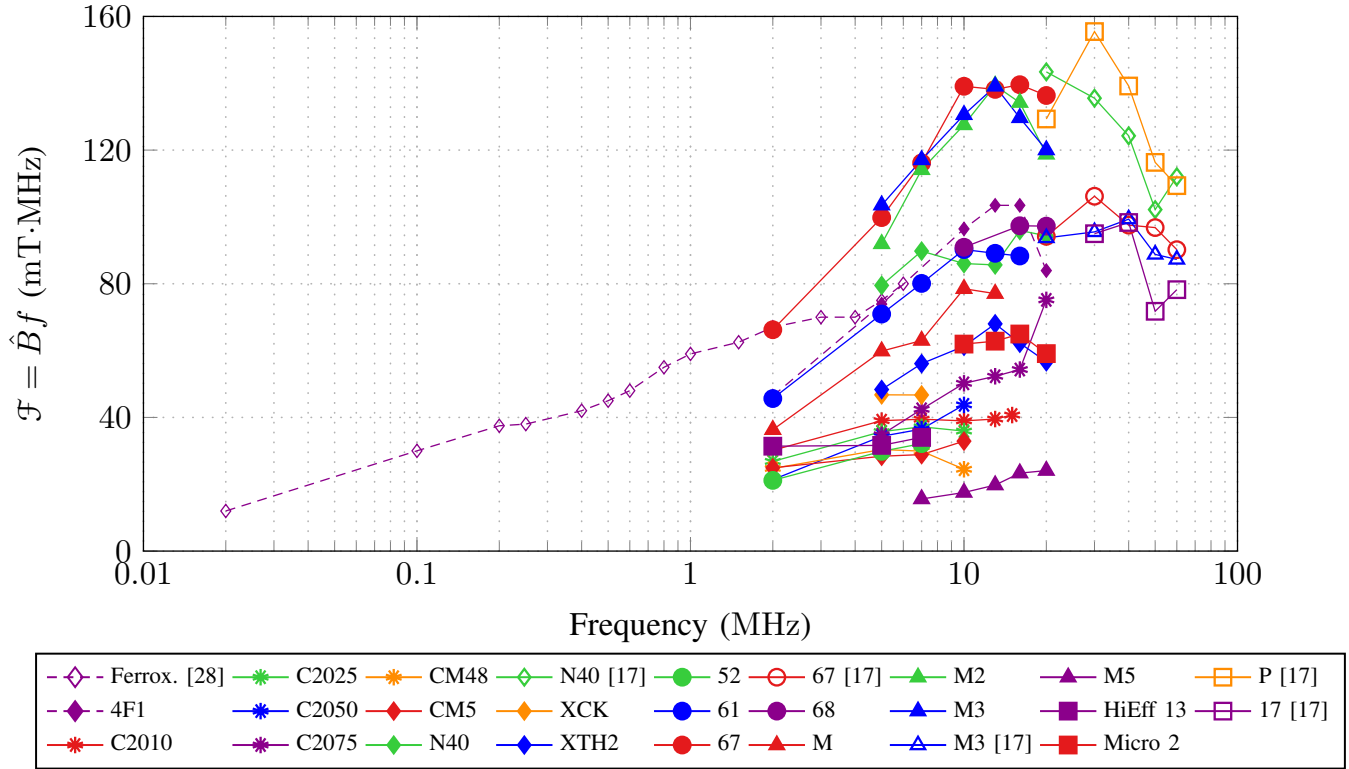


Fig. 2: Survey of standard performance factor, incorporating data from industry, the literature, and this work.

### Modified Performance Factor

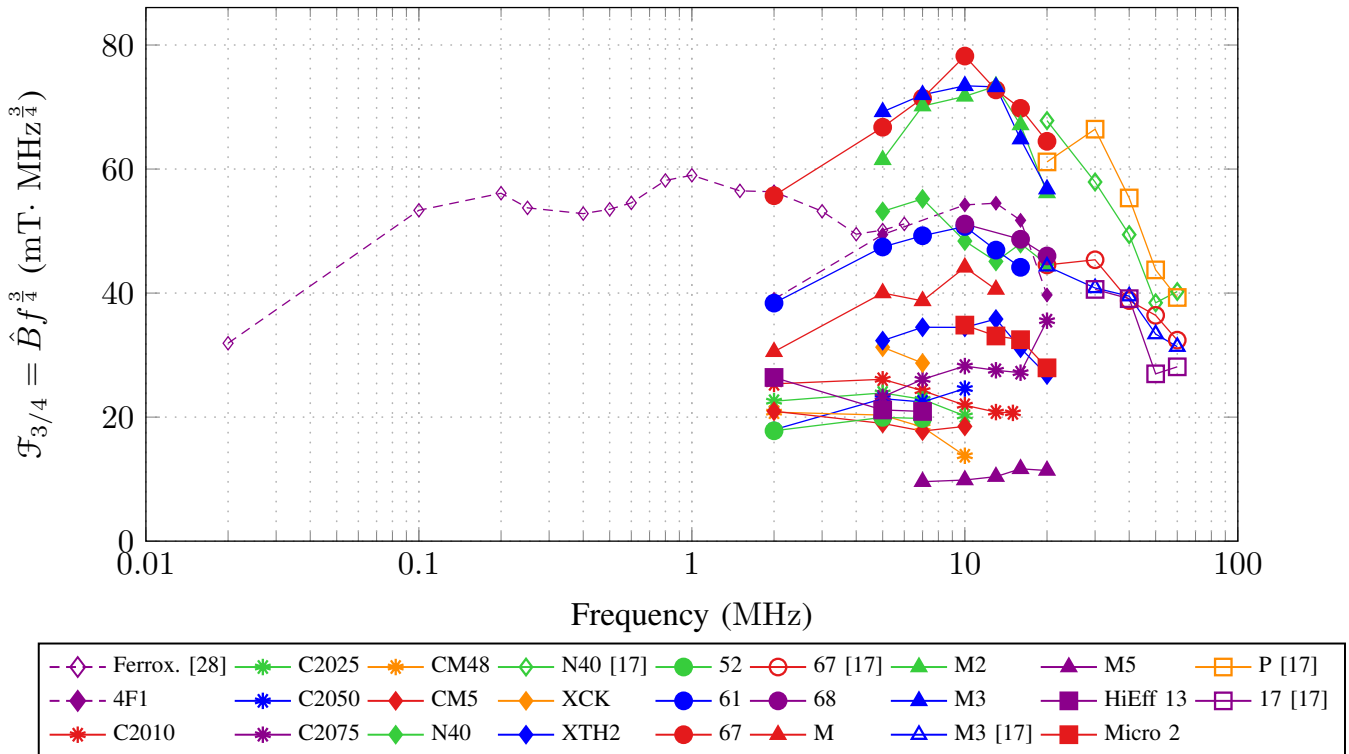


Fig. 3: Survey of modified performance factor, incorporating data from industry, the literature, and this work.

TABLE II: Steinmetz parameters measured in this work for commercially available materials at HF,  $P_v = k \times B^\beta$ , where  $P_v$  is in  $\text{mW}/\text{cm}^3$  and  $B$  is in  $\text{mT}$ ; valid for  $P_v < 1000 \text{mW}/\text{cm}^3$ .

Frequency→		2 MHz		5 MHz		7 MHz		10 MHz		13 MHz		16 MHz		20 MHz	
Material	$\mu_r$	k	$\beta$	k	$\beta$	k	$\beta$	k	$\beta$	k	$\beta$	k	$\beta$	k	$\beta$
Ceramic Magn. C2010 [39]	340	0.20	2.89	2.61	2.56	10.61	2.23	22.23	2.29	51.55	2.04	-	-	-	-
Ceramic Magn. C2025 [39]	175	0.49	2.67	3.14	2.58	11.33	2.27	30.15	2.20	-	-	-	-	-	-
Ceramic Magn. C2050 [39]	100	0.52	2.9	2.47	2.75	5.25	2.76	12.44	2.50	-	-	-	-	-	-
Ceramic Magn. C2075 [39]	50	-	-	2.31	2.77	3.42	2.77	5.81	2.76	11.88	2.69	20.67	2.61	19.57	2.45
Ceramic Magn. CM48 [39]	190	0.59	2.68	7.49	2.33	21.5	2.17	80.01	2.05	-	-	-	-	-	-
Ceramic Magn. CM5 [39]	290	0.61	2.66	9.42	2.29	22.55	2.19	42.04	2.08	-	-	-	-	-	-
Ceramic Magn. N40 [39]	15	-	-	1.52	2.09	3.04	2.00	6.61	2.01	11.09	2.02	12.47	2.06	21.20	2.04
Ceramic Magn. XCK [39]	210	-	-	1.07	2.75	4.86	2.44	-	-	-	-	-	-	-	-
Ceramic Magn. XTH2 [39]	80	-	-	0.83	2.82	1.72	2.72	3.86	2.68	7.07	2.57	15.20	2.57	42.00	2.38
Fair-Rite 52 [40]	250	0.46	2.97	5.44	2.53	14.44	2.32	-	-	-	-	-	-	-	-
Fair-Rite 61 [40]	125	0.08	2.79	0.42	2.67	0.83	2.62	1.80	2.56	4.31	2.47	6.66	2.53	-	-
Fair-Rite 67 [40]	40	0.10	2.44	0.69	2.20	1.11	2.18	2.09	2.08	2.91	2.18	6.06	2.04	10.95	1.99
Fair-Rite 68 [40]	16	-	-	-	-	-	-	3.92	2.2	-	-	11.71	2.08	22.67	1.96
Ferroxcube 4F1 [28]	80	0.15	2.57	1.11	2.27	-	-	2.86	2.28	6.53	2.09	10.89	2.05	23.20	2.14
Metamagnetics HiEff 13 [41]	425	0.11	3.06	10.44	2.10	12.69	2.32	-	-	-	-	-	-	-	-
Micrometals 2 [42]	10	-	-	-	-	-	-	10.97	2.09	19.32	2.07	28.79	2.04	57.09	2.00
National Magn. M [43]	125	0.03	3.36	0.45	2.83	1.35	2.69	2.52	2.57	5.23	2.56	-	-	-	-
National Magn. M2 [43]	40	-	-	0.41	2.44	0.69	2.36	1.45	2.3	2.85	2.18	5.39	2.13	12.58	2.07
National Magn. M3 [43]	20	-	-	0.85	2.10	1.66	2.03	2.55	2.05	4.87	1.95	7.54	2.01	14.44	1.98
National Magn. M5 [43]	7.5	-	-	-	-	90.34	2.14	147.6	2.17	198.3	2.21	225.1	2.12	335.1	2.15

TABLE III: Steinmetz parameters measured in [17] (reproduced here for completeness) for commercially produced materials at VHF,  $P_v = k \times B^\beta$ , where  $P_v$  is in  $\text{mW}/\text{cm}^3$  and  $B$  is in  $\text{mT}$ ; valid for  $P_v < 1000 \text{mW}/\text{cm}^3$ .

Frequency→		20 MHz		30 MHz		40 MHz		50 MHz		60 MHz		70 MHz	
Material	$\mu_r$	k	$\beta$										
National Magn. M3	20	0.0008	3.46	0.0068	3.24	0.191	2.45	1.03	2.15	1.76	2.11	-	-
Ferronics P	40	0.036	2.29	0.051	2.33	0.218	2.18	0.696	2.09	1.34	2.04	-	-
Fair-Rite 67	40	0.142	2.12	0.210	2.18	0.740	2.04	1.150	2.05	2.40	1.97	-	-
Ceramic Magn. N40	15	0.0364	2.23	0.227	2.02	0.518	2.00	0.208	2.58	0.690	2.25	-	-
Micrometals 17	4	-	-	0.0361	2.76	0.0825	2.72	1.860	2.10	1.95	2.16	2.35	2.22

frequency can be advantageous for reducing magnetics size, the benefits are not as large in this range. This is particularly true when winding loss is also considered, as reflected in the modified performance factor plotted in Fig. 3, where little if any benefit is seen in the 100 kHz to 2 MHz range.

However, both plots show substantial improvements above 2 MHz using some materials (e.g. Fair-Rite 67 and National Magnetics M2) that have not previously been widely used in power conversion applications. Moving from 2 MHz to 10 MHz, the best standard performance factor increases by a factor of approximately two, and the best modified performance factor increases by a factor of 1.45. Thus, for typical HF inductors or transformers with single-layer windings, we can expect a 45% increase in power density (in a power-loss-density limited design) to result from an increase in frequency from 2 MHz to 10 MHz. This same increase would also apply with an advanced winding technology limited by the number of winding layers. With a hypothetical winding technology that made skin and proximity effects negligible, without being constrained in the number of layers used or their thickness,

the full factor-of-two improvement would be available.

In order to illustrate the effect of operating frequency on magnetics size using a given core material, inductors were designed for constant impedance at various frequencies, allowing volume to scale to maintain  $Q$  constant. The inductors were designed with single-layer foil windings on ungapped cores in a low-permeability RF magnetic material (Fair-Rite 67,  $\mu_r = 40$ ), targeting an impedance of approximately  $35 \Omega$  with a quality factor of approximately 200, at a current handling of 1.6 A (ac peak). The results are demonstrated in Fig. 4. Ungapped inductors lack the degree of design freedom from the gap length and toroids are only available in certain fixed sizes, and therefore the illustrated designs are not fully optimized. However, the fact that the inductor loss is dominated by the core rather than the windings serves to highlight the *material* properties, and illustrates the general core selection tradeoffs. As can be seen in Fig. 4, the power density vs. frequency (at constant impedance and loss) improves significantly (by a factor of three) from the 3.5 MHz design to the 9 MHz design, but then quickly declines. Minimum inductor volume

(highest power density) is achieved in the frequency range where material performance factor peaks (compare Figs. 3 and 4).

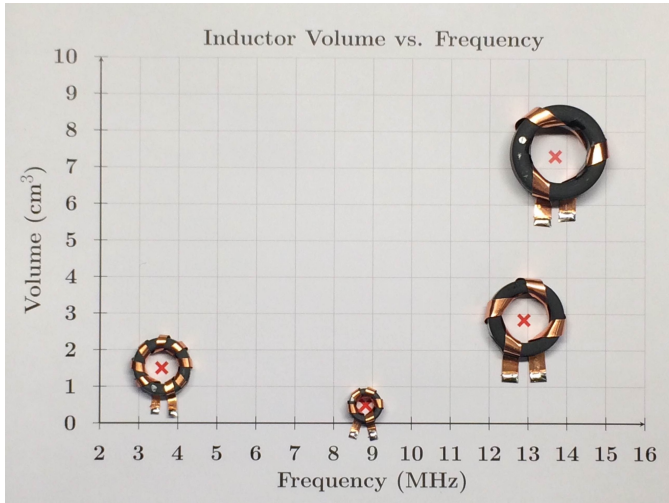


Fig. 4: Inductors using ungapped toroidal cores of Fair-Rite 67 material ( $\mu_r = 40$ ) designed for sinusoidal current at an impedance level of approximately  $35 \Omega$  and a quality factor of approximately 200 (see Table IV). The figure illustrates the inductor volume vs frequency at a given quality factor. Minimum inductor volume (highest power density) is achieved in the frequency range where material performance factor peaks.

TABLE IV: Power inductors designed for identical impedance and large-signal quality factor at an ac current of 1.6 A, corresponding to those in Fig. 4.

Frequency MHz	Impedance $\Omega$	Large-Signal Q	Volume $\text{cm}^3$	P/N
3.58	36.5	212	1.50	5967001801
8.83	33.7	193	0.49	5967001101
12.90	33.4	220	2.83	5967001001
13.70	39.9	202	7.33	5967002701

From this example we see that operating at frequencies best suited to a given magnetic material can offer significant benefit in power magnetic component design. Moreover, taken together with the data in Figs. 2 and 3, we can conclude that significant improvements in the power density of power magnetic components with cores (those that are limited in performance by core loss) can be achieved by moving into the HF regime (e.g., at least up to 10 MHz with available magnetic materials).

Improvements in main power stage magnetics are not the only advantages of higher-frequency operation for magnetic components and circuit design. For example, the size of magnetic components associated with filters (e.g., for EMI) are often not determined by core loss considerations, but rather by required filter cutoff frequency, such that increased operating frequency can yield very rapid reductions in component size (note that traditional nanocrystalline materials may still be used for EMI filters, as they typically require low-Q com-

ponents which are not limited by core loss and are allowed to be dissipative at the filtered frequencies). Since the EMI filter for a grid-interface converter can often consume 20% or more of system volume, frequency increases into the HF regime can help substantially reduce filter size and overall converter size. (This effect is illustrated in the design in [34], where EMI filter size is extremely small owing to operation in the 5–10 MHz range; indeed the volume of the entire converter is smaller than the required EMI filter alone for a typical 100 kHz-range design). Likewise, as illustrated in [2], increases in switching frequency (and the smaller associated inductance and capacitance values) can aid in substantially improving transient response speed of power converters.

## V. PERMEABILITY

Most magnetic materials suitable for HF operation have relatively low permeabilities ( $\mu_r < 250$ ), with some of the highest performance factors achieved with  $\mu_r \approx 40$  (Fig. 5). High relative permeability  $\mu_r$  is sometimes thought to be important for the design of magnetic components; however, neither the traditional performance factor  $\mathcal{F}$  nor the modified performance factor  $\mathcal{F}_{\frac{3}{4}}$  directly depend on the material permeability. It is natural to inquire whether the low-permeability materials available are effective in practice for power magnetic component designs at HF, whether there is some sacrifice made by using low permeability materials in general, and the extent to which permeability can be reduced before design becomes problematic. In this section we demonstrate that, in general, only very modest permeabilities are needed for effective magnetics design and that higher permeabilities cease to improve performance.

### A. In Inductors

The impact of permeability may be shown most easily for the case of an inductor with a target impedance. The inductance of an ungapped inductor is given by

$$L_{\text{ungapped}} = \frac{N^2}{\mathcal{R}_{\text{core}}} = \frac{\mu_0 \mu_r N^2 A_c}{l_c} \quad (3)$$

where  $\mathcal{R}_{\text{core}}$  is the core reluctance,  $N$  is the number of turns,  $A_c$  is the core cross-sectional area, and  $l_c$  is the flux path length through the core (Fig. 6 with  $l_g = 0$ ). From (3) one may surmise that a higher  $\mu_r$  could be directly traded for lower  $N$  to reduce copper loss at little or no expense. However, achieving minimum loss in an inductor almost always requires a *gapped inductor* to reduce core loss [48]. With a high permeability material, the reluctance in the flux path is usually dominated by the gap, and the inductance is approximated by

$$L_{\text{gapped}} \approx \frac{N^2}{\mathcal{R}_{\text{gap}}} = \frac{\mu_0 N^2 A_g}{l_g} \quad (4)$$

where  $\mathcal{R}_{\text{gap}}$ ,  $A_g$  and  $l_g$  are the *gap* reluctance, cross-sectional area and length respectively. Here it is clear that permeability has little influence on design.

However, with lower permeability materials like the high-performance materials in Fig. 5, the reluctance of the gap may

### $\mathcal{F}$ by Permeability

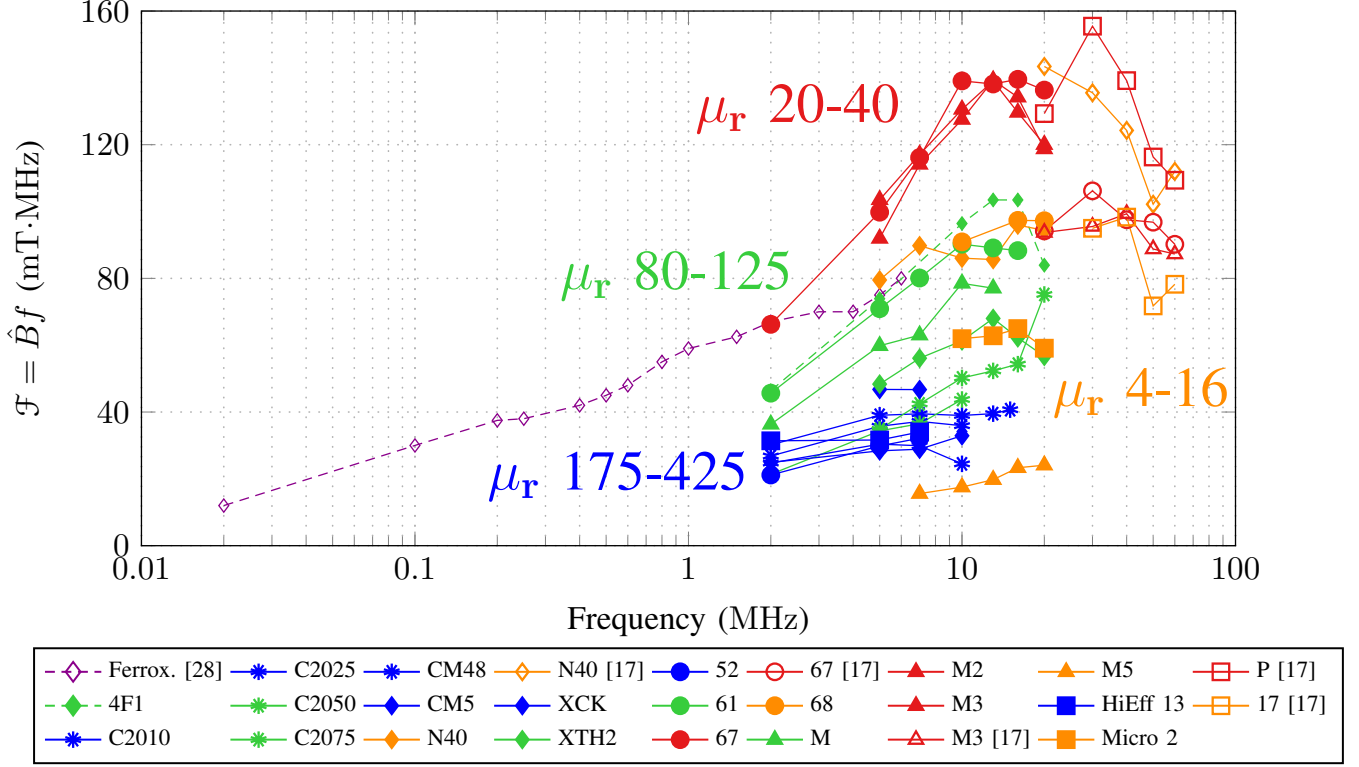


Fig. 5: Performance factor sorted by permeability. Curves shown in orange are for relative permeabilities of 4–16, those in red are for relative permeabilities of 20–40, in green for relative permeabilities of 80–125 and in blue for relative permeabilities of 175–425. It can be seen that materials having permeabilities of 20–40 often have the highest performance factor in the HF range.

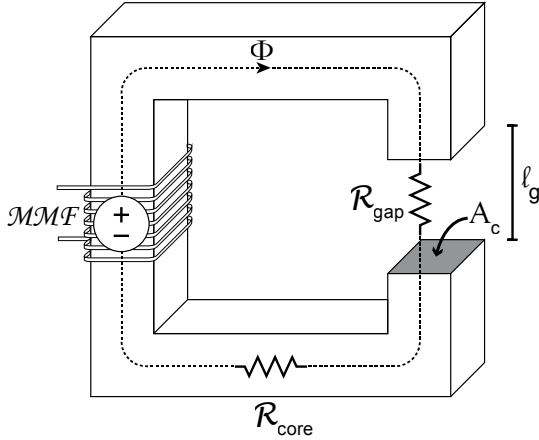


Fig. 6: Magnetic Circuit for Inductors

not be completely dominant, and the inductance is given by

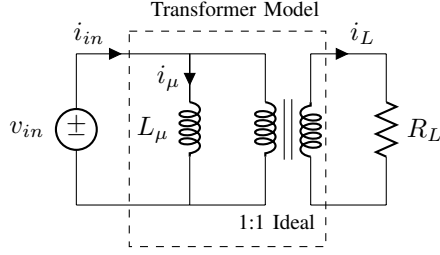
$$L_{gapped} = \frac{N^2}{\mathcal{R}_{tot}} = \frac{\mu_0 N^2 A_g}{l_g + \frac{l_c}{\mu_r}} \quad (5)$$

From (5) we see that as permeability decreases,  $l_g$  must also decrease in order to maintain the same inductance (if, hypo-

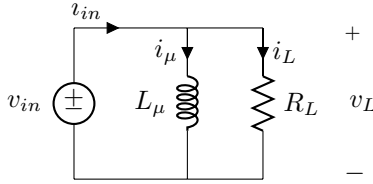
thetically, permeability could be varied independently of other material parameters). Doing so also maintains the same flux density. Thus, the performance is not affected by the reduction in permeability until the required gap length reaches zero. Further decreases in permeability cannot be accommodated by adjusting the gap length, and so the desired balance between core loss and winding loss cannot be maintained—an increase in the number of turns is needed in order to maintain the inductance, and this necessitates an increase in winding loss. Thus there is a permeability threshold above which further increases in permeability change the gap size but do not affect performance. Below that point, decreases in permeability do hurt performance because of the increase in  $N$  needed to maintain inductance. The threshold permeability is simply that which provides the specified inductance with a number of turns that provides a good tradeoff between core loss and winding loss without a gap. Based on (3), the threshold permeability is given by

$$\mu_{r,threshold} = \frac{Ll_c}{\mu_0 N^2 A_c} \quad (6)$$

Thus we see diminishing returns on increasing permeability in the design of inductors. In this case, the advantage of additional permeability decays to zero at a finite value of permeability,  $\mu_{r,threshold}$ .



(a) Transformer circuit with transformer model.



(b) Simplified Transformer Circuit

Fig. 7: Transformer circuits used to examine achievable power density and its relationship to performance factor and permeability.

### B. In Transformers

The principle of diminishing returns on permeability can be observed through a different lens by examining the case of a transformer. For simplicity, consider a sinusoidally driven 1:1 transformer with a single-layer winding driving a resistive load, as in Fig. 7 where we have included the magnetizing inductance  $L_\mu$  and neglected leakage inductances. Let the peak magnetic flux density be limited to a value  $\hat{B}$ , as in the definition of performance factor. Further, let the surface current density in the windings be limited to  $\hat{K} = NI_{in}/l_c$ . The average power delivered to the load is given by

$$P_{del} = \frac{1}{2} V_L I_L \quad (7)$$

where capital symbols such as  $V_L$  and  $I_L$  represent the peak of the respective voltage and current waveforms. The peak load voltage is limited by the allowed magnetic flux density induced in the magnetizing inductance. The relationship is given by Faraday's law:

$$V_L = V_{in} = \omega N A_c \hat{B} \quad (8)$$

The load current is related to the total current by

$$I_L = \sqrt{I_{in}^2 - I_\mu^2} \quad (9)$$

where  $I_\mu = V_{in}/(\omega\mu L_\mu)$  is the peak current through the equivalent magnetizing inductance.

Thus the power deliverable to the load with constraints on magnetic flux density and surface current density is given by

$$P_{del} = \frac{1}{2} V_L I_L = \frac{1}{2} \omega N A_c \hat{B} \sqrt{\left(\frac{\hat{K} l_c}{N}\right)^2 - \left(\frac{l_c}{N^2 \mu A_c \omega}\right)^2} \quad (10)$$

This can be rearranged and expressed in power per unit core volume as:

$$\begin{aligned} \frac{P_{del}}{A_c l_c} &= (\pi \hat{K}) (\hat{B} f) \sqrt{1 - \left(\frac{\hat{B}}{\hat{K} \mu}\right)^2} \\ &= (\text{Constant})(\mathcal{F})(\text{Correction Factor}) \quad (11) \end{aligned}$$

where the volumetric power handling is shown proportional to the traditional performance factor  $\mathcal{F} = \hat{B} f$  quite naturally. In fact, (11) contains within it the modified performance factor as well. For example,  $\hat{K} \propto \hat{K}_0 f^{-1/4}$  would account for skin effect in the same winding at high frequency, which produces  $\hat{B} f^{3/4} = \mathcal{F}_{3/4}$  in the expression for deliverable power density.

Equation (11) demonstrates another context for the principle of diminishing returns on permeability. For a transformer, the permeability both guides flux and increases the magnetizing impedance. However, increasing the shunt impedance of the magnetizing inductance is only important when  $|Z_\mu| = L_\mu \omega \sim R_L$ . Once  $|Z_\mu| \gg R_L$ , the benefit saturates and additional permeability cannot significantly improve component performance. The correction factor in (11) approximates to 1 and drops out of consideration.

In order to show that the correction factor  $\sqrt{1 - \left(\frac{\hat{B}}{\hat{K} \mu}\right)^2} \approx 1$  even for HF ferrites with low permeabilities, it is necessary to set values for  $\hat{B}$  and  $\hat{K}$ . This is equivalent to choosing the balance of core loss and copper loss. For a fixed total loss budget  $P_{loss}$  (as would be the case for efficiency or temperature-rise limited components), the allowed magnetic flux density and current density are related to each other:

$$P_{loss} = P_{core}(\hat{B}) + P_{cu}(\hat{K}). \quad (12)$$

The copper loss,

$$P_{cu} = \frac{1}{2} I_{in}^2 R_{cu} \quad (13)$$

is specified by the total winding resistance in terms of the turn length  $l_w$  and the width of one (e.g. foil) turn  $w$ ,

$$R_{cu} = \rho \frac{N l_w}{w \delta} = \rho \frac{N^2 l_w}{l_c \delta} \quad (14)$$

assuming a single-layer winding distributed around the full perimeter of the core,  $l_c$ , in the skin-depth limit. This yields:

$$P_{cu} = \frac{1}{2} I_{tot}^2 \rho \frac{N^2 l_w}{l_c \delta} = \frac{1}{2} \hat{K}^2 \rho \frac{l_c l_w}{\delta}. \quad (15)$$

The core loss is given by the Steinmetz parameters measured in Section III:

$$P_{core} = A_c l_c k_f \hat{B}^\beta. \quad (16)$$

An approximate relationship between  $\hat{B}$  and  $\hat{K}$  can be found by setting core loss and copper loss equal to each other. While this does not guarantee maximum delivered power for a given loss budget (or maximum efficiency for given power handling), it usually provides a first-order approximation [48]. The resulting relationship is:

$$\frac{\hat{B}^{\beta/2}}{\hat{K}} = \sqrt{\frac{\rho l_w}{2 A_c k_f \delta}}. \quad (17)$$

The exact expression can also be used,

$$\hat{K} = \sqrt{(P_{loss} - A_c l_c k_f \hat{B}^\beta) \frac{2\delta}{\rho l_c l_w}}. \quad (18)$$

Given the constraint relating  $\hat{B}$  to  $\hat{K}$ , the best choice of  $\hat{B}$  and  $\hat{K}$  is the combination of values which maximize delivered power. To select  $\hat{B}$  and  $\hat{K}$ , therefore, it is necessary to plug either (17) or (18) into (11) and find the maximum of  $P_{del}$  numerically.

To conceptually illustrate the effect of permeability on component performance, we carry out a thought experiment by considering an ensemble of hypothetical core materials with identical loss characteristics but different permeabilities<sup>2</sup>. We consider a thermally-limited design using the parameters from Table V, with a total volume of  $1 \text{ cm}^3$ . We also use loss parameters equal to those of Fair-Rite 67 at 10 MHz. As will be shown, even if we could select among identical materials with arbitrary permeabilities, the benefit of high permeability saturates above a certain (typically low) value.

We begin with a traditional design, which assumes that the magnetizing inductance  $L_\mu$  is very large, and therefore the magnetizing current  $I_\mu$  is negligible. This is equivalent to assuming that the material permeability is very high (i.e. using a material from our ensemble with very high permeability). We carry out our design, maximizing the deliverable power density (11) for the temperature rise given in Table V. We then substitute into our design our other cores with identical geometries and loss characteristics, but less and less permeability. We do not re-optimize our design as permeability is decreased, but continue to use the same  $\hat{B}$  and  $\hat{K}$  that we calculated for our original design. As permeability is decreased, the component achieves less and less deliverable power for the available temperature rise, owing to the increase in magnetizing current. The ratio of achieved power density to the maximum achievable power density (i.e. for the highly permeable material) is then calculated and denoted the *un-optimized power ratio*  $\mathcal{P}$ <sup>3</sup>. The result for our thought experiment is plotted in Fig. 8. It can immediately be seen that reduced permeability is only problematic below a certain point. We notice almost no change as we reduce permeability from  $\mu_r \gg 100$  all the way to  $\mu_r = 100$  (not shown). Our (hypothetical) measurement equipment begins to detect a small loss in performance as we go from  $\mu_r = 100$  to  $\mu_r = 50$ , and our component continues to incur less than 10% performance loss as permeability drops to  $\mu_r \approx 22$ . Below  $\mu_r \approx 22$ , performance collapses until the temperature budget is used up by the loss due to the magnetizing current alone and no power can be delivered to the load. It can also be seen that, although

<sup>2</sup>This is equivalent to imagining that we can vary a single core material's permeability independent of other material properties. While this, in general, is not practical (permeability is influenced by the same micro-structural factors that determine material loss characteristics), in principle we may vary permeability in isolation and investigate its effect on design.

<sup>3</sup>Note that this ratio is equal to the correction factor in this case. This leads to one possible physical description of the correction factor: the correction factor is the ratio of a magnetic component's power density achievable with a low-permeability material to that achievable with an otherwise identical high-permeability material, if the design points  $\hat{B}$  and  $\hat{K}$  are maintained from the high-permeability design in both cases.

TABLE V: Parameters for Power Ratio Calculations

Outer Diameter	scale $\times$ 22.1 mm
Inner Diameter	scale $\times$ 13.7 mm
Thickness	scale $\times$ 6.35 mm
Temperature Rise	50 °C
Thermal Law [2]	$P_{loss} = 0.0475 \times \text{Surface Area (cm}^2) \times \Delta T$ (°C)
Frequency	10 MHz

Variable Permeability Thought Experiment

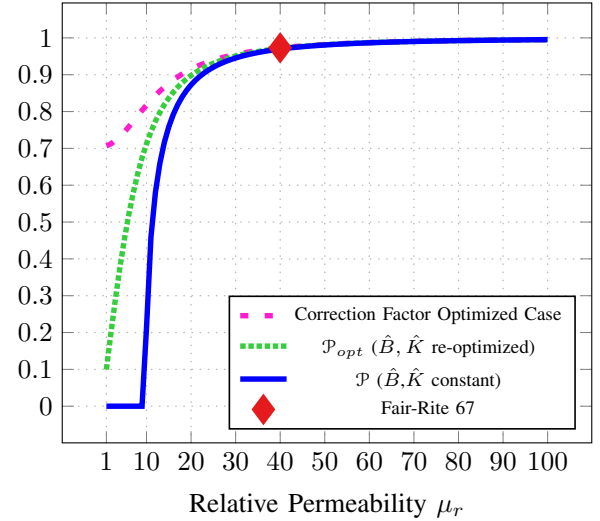


Fig. 8: A theoretical ensemble of materials with the same material loss parameters but different permeabilities. Each point represents an optimization with (11) maximized using the parameters in Table V with a volume of  $1 \text{ cm}^3$ . The deliverable power, normalized to a high-permeability design, is plotted where  $\hat{B}$  and  $\hat{K}$  are held constant ( $\mathcal{P}$ ). The same ratio is also plotted with re-optimized designs ( $\mathcal{P}_{opt}$ ), along with the correction factor for this case. The loss parameters used match those of Fair-Rite 67 at 10 MHz; its permeability ( $\mu_r = 40$ ) is noted on the graph.

Fair-Rite 67 (a real material with the same loss parameters) only has a permeability of  $\mu_r = 40$ , that permeability is ample to provide the available benefit of the magnetic core.

These conclusions are actually overly pessimistic; the picture improves if we *do* re-optimize each design as we decrease permeability. This experiment follows as before, but the operating points  $\hat{B}$  and  $\hat{K}$  are re-optimized at each permeability to maximize (11). The achievable power in this case is also normalized to the achievable power with a high-permeability material and the ratio is denoted the *optimized power ratio*  $\mathcal{P}_{opt}$ . The results are plotted in Fig. 8; it can be seen that  $\mathcal{P}_{opt}$  falls off less sharply as permeability is decreased than the un-optimized case  $\mathcal{P}$ . For example, a properly designed component at  $\mu_r = 10$  (significantly lower than  $\mu_r \approx 22$ ) would still provide substantial power delivery while an un-optimized design would have lost all utility at that permeability.

The reason for this improvement lies in the interaction between the  $\hat{B} \cdot \hat{K}$  product and the correction factor in (11). The correction factor is plotted in Fig. 8 for the previous experiment where each design was re-optimized to select  $\hat{B}$

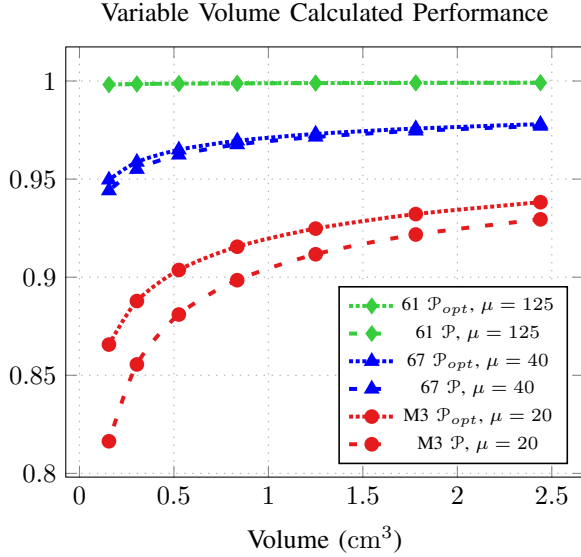


Fig. 9: Un-optimized and optimized power ratios ( $\mathcal{P}, \mathcal{P}_{opt}$ ) for example materials and volumes. Parameters in Table V.

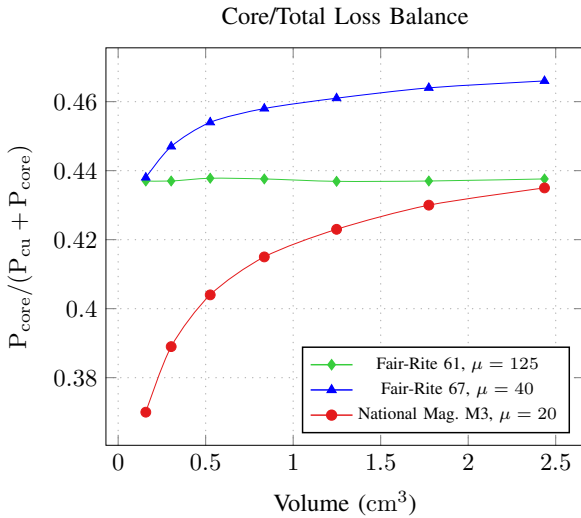


Fig. 10: The fraction of total loss attributable to core loss for example materials and volumes for the optimized case as in Fig. 9. Parameters in Table V.

and  $\hat{K}$  to maximize power delivery. The plot for the first case, where designs were not re-optimized, is already its own correction factor since none of the other factors were allowed to vary. It can be seen that, without re-optimization, the deliverable power collapses at low permeability due to the correction factor, whereas re-optimization at low permeability trades lower  $\hat{B}$  for higher  $\hat{K}$  to keep the correction factor high. In that case the deliverable power still drops because both the  $\hat{B} \cdot \hat{K}$  product and correction factor are reduced slowly, but the collapse is not as severe.

Based on this thought experiment, it may be concluded that practical designs can achieve high power density with relatively modest permeabilities. This is because, holding other factors constant, increasing permeability above fairly low val-

ues provides greatly diminishing returns of achievable power density. The principle of diminishing returns on permeability is demonstrated for some real materials by calculating  $\mathcal{P}_{opt}$  and  $\mathcal{P}$  using the parameters in Table V and allowing volume to vary while maintaining the geometric ratios; the results are plotted in Fig. 9. Several conclusions may be drawn from the curves in Fig. 9. First,  $\mathcal{P}_{opt}$  falls farther below 1 the lower the permeability of the material, as one would expect. Second, the lower the permeability, the greater the variation between  $\mathcal{P}$  and  $\mathcal{P}_{opt}$ , in the same way that their values diverge at low permeability in Fig. 8. Third, as volume is decreased there is both a decline in achievable performance and a greater deviation of  $\mathcal{P}$  from  $\mathcal{P}_{opt}$ . Finally, despite all of these effects, in most cases<sup>4</sup> the power ratios for low permeability materials are above 0.9, indicating that permeability has a small influence on performance. Additionally, the balance of core loss and total loss for the optimized case is plotted in Fig. 10, and is consistent with the general rule that minimizing total loss usually requires core loss to be equal to or slightly less than copper loss [49]. Little is sacrificed, and much is gained, by using high-performance materials with low permeabilities at HF.

## VI. CONCLUSION

The drive to increase frequency in power conversion circuits, enabled by advanced circuit designs and wide-band-gap semiconductors, is primarily predicated on the idea that passive components can be made smaller and cheaper, and that systems can achieve higher performance. The extent to which power magnetic components can be improved at higher frequencies hinges on their loss behavior over frequency. Determining this requires information on the loss characteristics of the available magnetic materials. We have undertaken measurements to produce the necessary data, and the results suggest that significant improvements in performance are possible through operation at HF using commercially available magnetic materials. Performance factor and modified performance factor facilitate understanding the implications of these data for selecting an operating frequency and understanding what is achievable. Finally, we conclude that an upper bound exists on the amount of relative permeability necessary to develop optimized magnetic-core designs, and that for many designs the low permeability of available low-loss materials is not a disadvantage.

## APPENDIX A PERFORMANCE FACTORS FOR OTHER WINDING CONFIGURATIONS

In Section II, we discussed formulations of the performance factor that are appropriate for a variety of winding conditions (see Table I). We have focused on the standard performance factor  $\mathcal{F}_1$  as a reference and the modified performance factor

<sup>4</sup>Most of the materials with high performance from Figs. 2 and 3 have  $\mu_r \geq 20$ , and designs at most power levels will use components larger than  $0.5 \text{ cm}^3$ . Additionally, the thermal model used overestimates temperature rises [2], especially as volume decreases. The performance degradation at low volumes in Figs. 9 and 10 would likely not be as severe in practice.

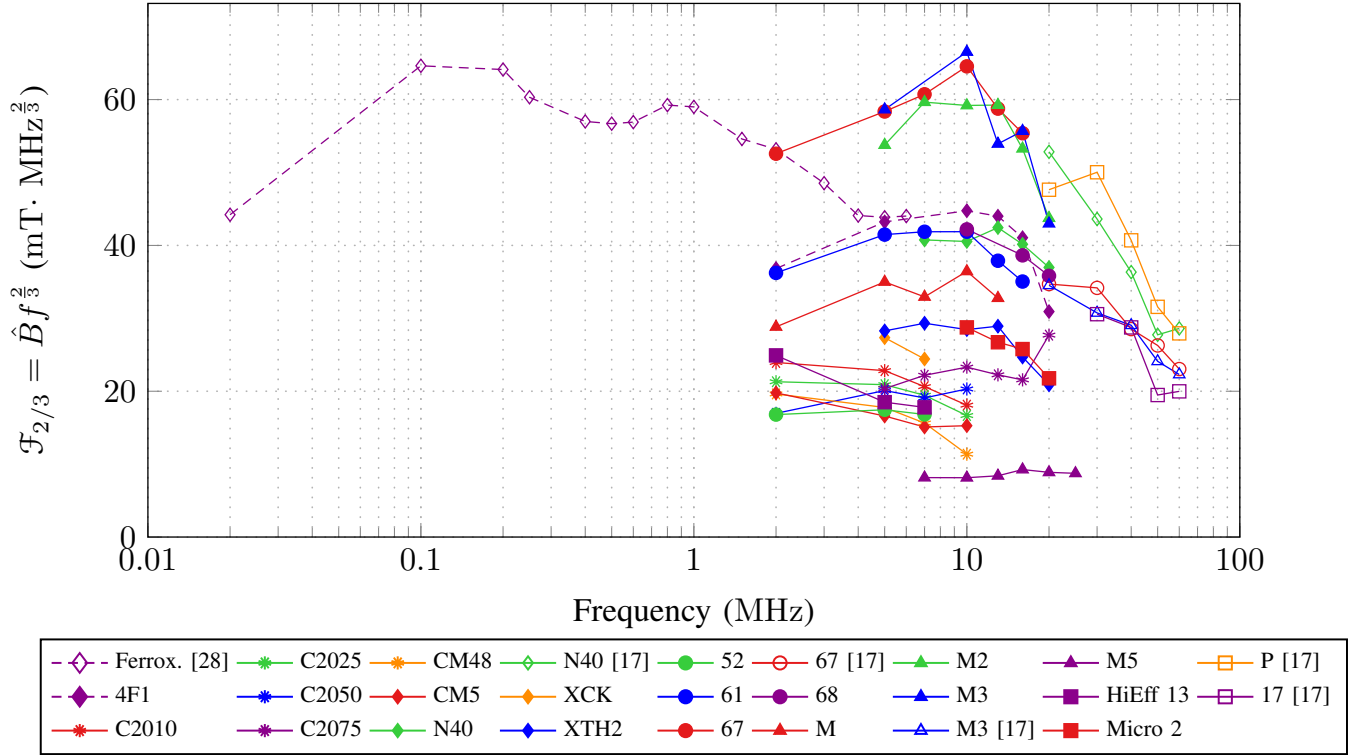


Fig. 11: Survey of  $\mathcal{F}_{2/3}$ , incorporating data from industry, the literature, and this work.

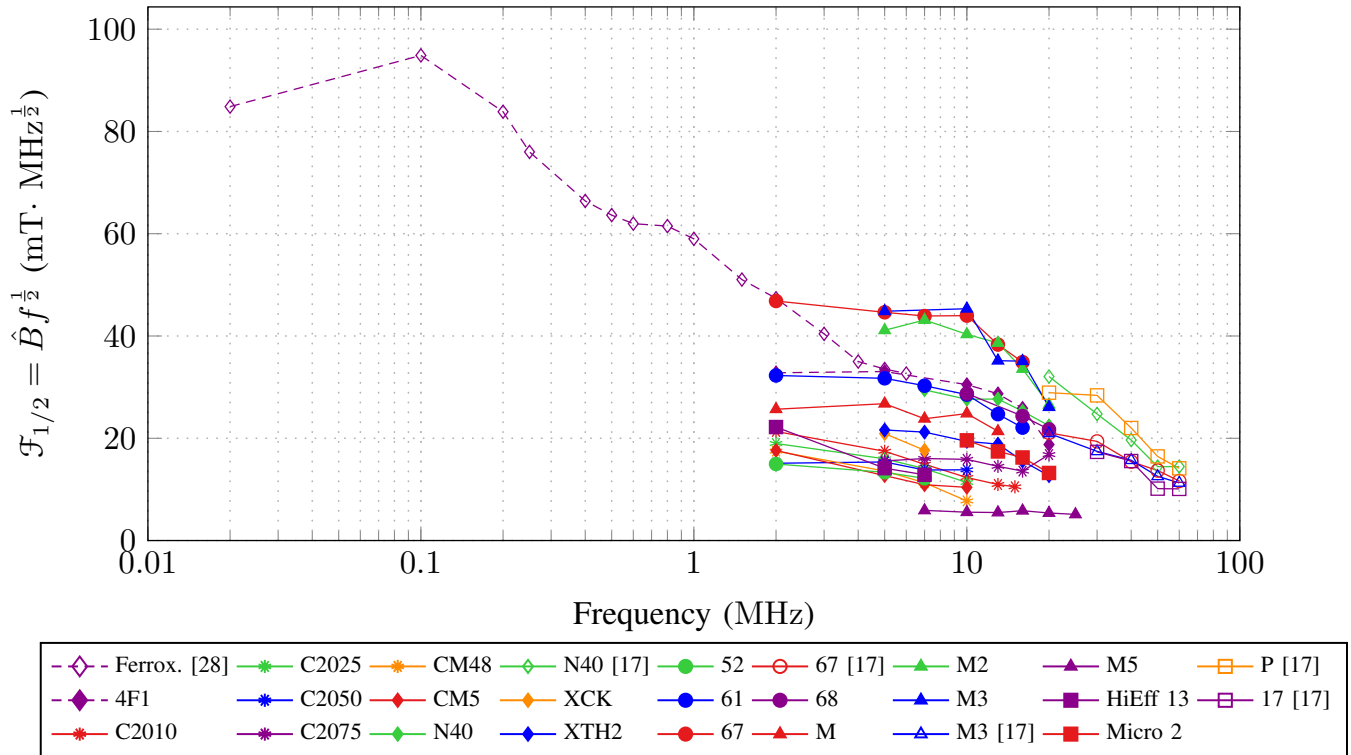


Fig. 12: Survey of  $\mathcal{F}_{1/2}$ , incorporating data from industry, the literature, and this work.

corresponding to a single layer winding  $\mathcal{F}_{\frac{3}{4}}$  as the most likely scenario for HF design. For completeness, we include in Figs. 11–12 the calculated performance factors corresponding to a fixed layer thickness  $\mathcal{F}_{\frac{1}{2}}$  and to a fixed number of wire strands  $\mathcal{F}_{\frac{2}{3}}$  based on the same data.

Fig. 11 shows  $\mathcal{F}_{\frac{2}{3}}$ , which is appropriate when the number of litz strands is a constraint. It indicates similar performance with novel materials at HF and with materials near 100 kHz. However, this scenario is unlikely to be realistic over this full frequency range, given that the required strand diameter in the HF range would not likely be practical. Fig. 12 shows  $\mathcal{F}_{\frac{1}{2}}$ , which is appropriate when a multilayer winding with fixed layer thickness and the optimum number of strands or layers is used. It indicates rapidly declining performance as frequency is increased past about 100 kHz. However, the assumptions limit the applicability of this result. If a relatively large layer thickness must be used, the high-frequency designs would perform better with single-layer windings, which result in the trend shown in Fig. 3 corresponding to  $\mathcal{F}_{\frac{3}{4}}$ . If a relatively small layer thickness is used, designs in the 100 kHz range would require an impractically large number of layers or strands and an impractically large window area. Once the window area constraint becomes the limiting factor, the trend approaches that of conventional performance factor  $\mathcal{F}_1$  (Fig. 2).

## APPENDIX B CORE LOSS MEASUREMENT METHODS

Core loss measurement approaches may be divided into calorimetric methods [50]–[56] and electrical methods, which include the classical two-winding method [48], [50]–[52], [57], [58] and resonant techniques [17], [59]–[62]. The two-winding method is sensitive to phase errors, which become increasingly difficult to control at higher frequencies. Phase errors can be reduced by adding a resonant capacitor to the drive winding and using the sum of the sense winding voltage and the capacitor voltage for the voltage measurement [59], [61]. A variation on this approach uses an air-core transformer in place of the capacitor to cancel the reactive component over a wider frequency range [60], [61]. Although the sensitivity to phase error is reduced by the methods of [59]–[61], the phase information is still necessary in the measurement. An alternative to two-winding methods is the resonant  $Q$  measurement approach in [17]. Either approach can be accurate in the HF range, but in the resonant  $Q$  approach phase measurement is not required, eliminating that source of error.

For the above reasons, we elected to use the resonant  $Q$  approach from [17], since it is suitable for accurate measurements in the HF range. The measurement setup consists of an RF power amplifier source in series with a high- $Q$  resonant tank, as in Fig. 13. Due to the low impedance of the measurement circuit at resonance, a 50  $\Omega$  to 3  $\Omega$  transmission line transformer (AVTECH AVX-M4) is used to better match the output impedance of the power amplifier. A low- $Q$  parallel resonant filter is also added to remove any harmonic components from the input to the measurement circuit. These components are simply added to ensure that the input voltage to the measurement circuit is a single-frequency sinusoid. As

will be described, the measurement itself only depends on  $v_{in,pk}$  and  $v_{out,pk}$ , so the actual implementation to the left of the dotted line in Fig. 13 is immaterial so long as good drive waveform quality is obtained.

The voltage at the input to the tank and the output voltage (i.e. the voltage across the resonant capacitor) are measured with respect to ground. At the undamped resonant frequency  $\omega_r = 1/\sqrt{LC}$  the quality factor of the inductor is simply the ratio of the output to the input voltage amplitudes

$$\begin{aligned} \frac{V_{out-pk}}{V_{in-pk}} &= \left| \frac{R_C + \frac{1}{j\omega_r C_m}}{R_{core} + R_{cu} + R_C} \right| \approx \frac{\omega_r L_m}{R_{core} + R_{cu}} \\ &= Q_{L_m} \end{aligned} \quad (19)$$

where  $R_C$  is the equivalent series resistance (ESR) of the capacitor, and  $R_{cu}$  and  $R_{core}$  are equivalent series resistances representing winding (copper) loss and core loss, respectively. In the above derivation, the reactance of the capacitor cancels that of the inductor at the resonant frequency. The approximation is also made that the capacitor equivalent series resistance is small with respect to the modeled inductor resistance.

The circuit resistance modeling core loss can be calculated from measured values

$$R_{core} = \frac{2\pi f_s L V_{in-pk}}{V_{out-pk}} - R_C - R_{cu} \quad (20)$$

where the copper resistance is estimated from measurements of an air-core inductor of identical construction and/or through numerical modeling. The current through the inductor and capacitor is the same (and known from the measured  $V_C = V_{out}$ ) so volumetric power loss can be computed directly:

$$P_V = \frac{I_{L-pk}^2 R_{core}}{2V_L} \quad (21)$$

Possible sources of error and mitigation strategies are covered in [17]. This approach can yield core loss measurements that are accurate to better than 20%, which is sufficient for design purposes and within the lot-to-lot variation of typical materials.

## APPENDIX C DC EFFECTS

There are several factors which limit the applicability of the Steinmetz equation to losses in practical power converters. While loss characteristics for magnetic materials are measured and reported for sinusoidal ac magnetic flux densities (equivalently, sinusoidal ac currents), these waveforms are only encountered for a small subset of power converter topologies (e.g. resonant converters). Magnetic components often have magnetizing currents with significant harmonic components, such as triangular or trapezoidal waveforms, and may have significant dc components (e.g. in continuous conduction mode buck or boost converters). It is known that harmonic content increases core loss beyond that predicted by summing the loss contributions of each harmonic in a waveform (an incorrect approach, due to the non-linear nature of material core loss). Nevertheless, several well-justified approaches have been developed to accurately account for such losses [63]–[66].

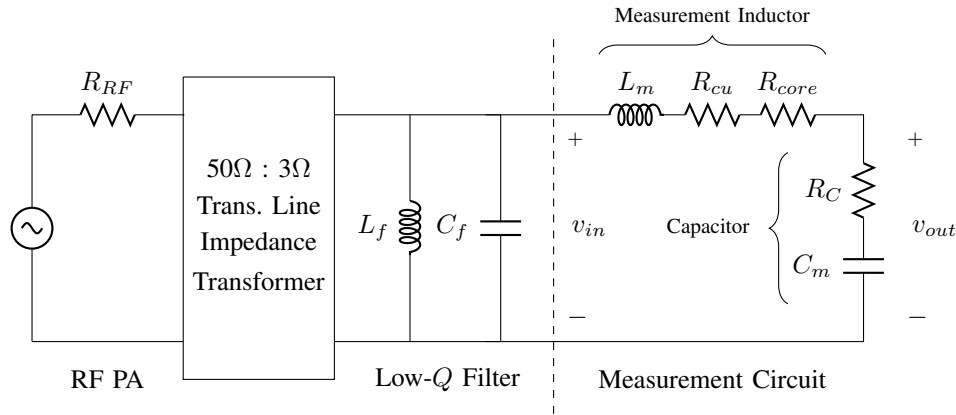


Fig. 13: Circuit schematic used for core loss measurement.

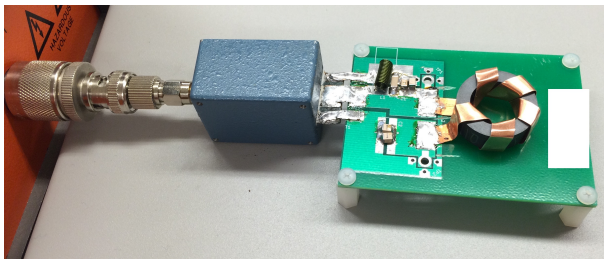


Fig. 14: Image of a test circuit in operation. The power amplifier (orange, left) connects to the board through the transmission line transformer (blue). The input filter, measurement inductor, and resonant capacitor are visible.

It is also known that waveforms with significant dc components lead to higher core losses than otherwise identical waveforms without any bias, despite the fact that the dc component does not cause dynamic dipole rotation or domain wall motion. These effects have been documented, but no general theory (neither empirical nor from first principles) exists to allow designers to take this effect into account. It should be noted that this effect is independent from concerns about core saturation, and occurs even when peak flux densities are well below saturation.

We investigated the effect of dc bias on core loss for NiZn materials in the HF regime, and found that core loss typically increased substantially with large superimposed dc magnetic flux densities. Measurements with dc bias were done using the same test setup as in Fig. 13 with modifications to provide a flux bias to the core. A secondary winding was applied to the measurement inductor, and a dc power supply was used to apply a constant current through the secondary winding to impose a dc flux density bias on the core (see Fig. 15). Two large air-core inductors (designed according to the guidelines in [67]) were placed in series with the secondary winding in order to provide a constant current through it while not exposing the power supply to high voltages due to transformer coupling from the resonant measurement circuit. An ac flux density was applied to the core, and the dc bias was varied in both positive and negative directions. The change in loss was measured, and the change in inductance

(i.e. effective permeability) was inferred from the change in resonant frequency. The results are shown in Figs. 16 and 17. Loss increases and inductance changes are substantial, and show significant hysteresis which make such effects difficult to account for in dynamic operation.

It can be seen that flux density waveforms with significant dc components can result in large undesirable effects which are difficult to model and predict. Therefore, designers should be aware that, greatly increased core losses may result in magnetic components with NiZn ferrites at HF in designs having large dc bias levels. One useful heuristic is to design such that the dc component is on the same order or less than the tolerable ac magnitude since loss was not observed to escalate under these conditions. For the general case it is unknown whether the dc value alone or its ratio to the ac magnitude is (most) important.

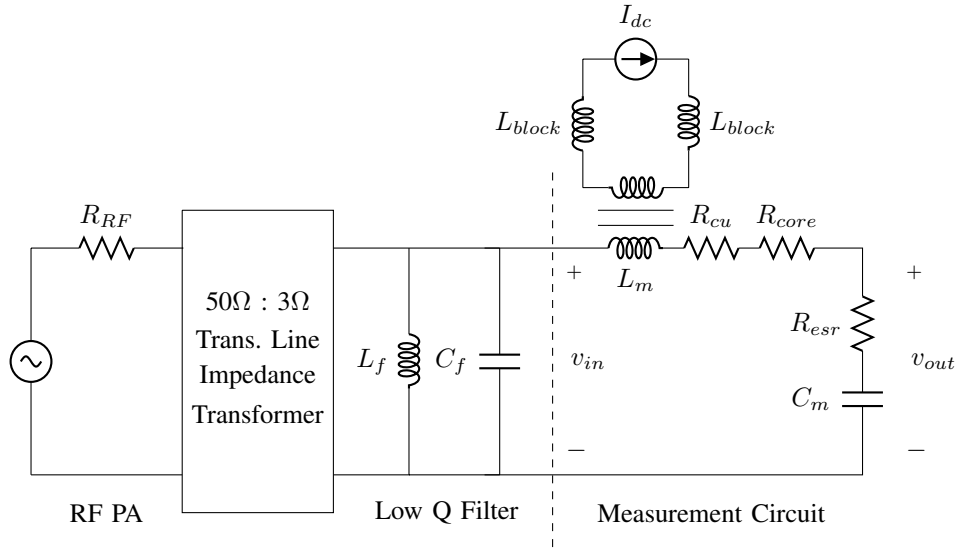


Fig. 15: Measurement circuit for evaluating material performance with both ac flux and superimposed dc bias.

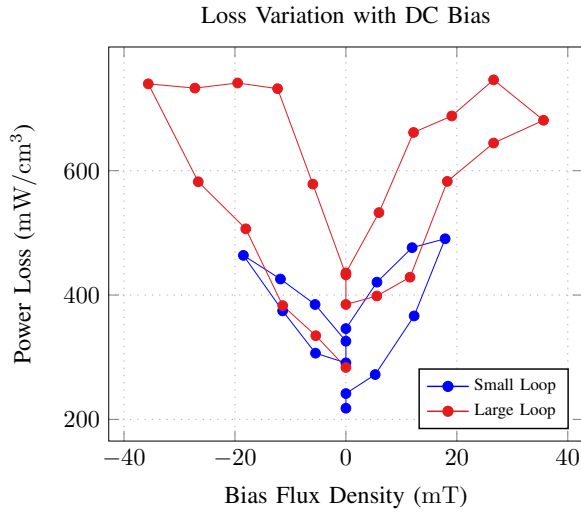


Fig. 16: Core loss increase of National Magnetics M ( $\mu_r = 125$ ) at 10 MHz with ac flux swing held constant at 6.5 mT and dc bias slowly changing. The small loop experiment was conducted first, followed by the large loop. Bias flux can increase loss density by at least a factor of three, with significant hysteresis.

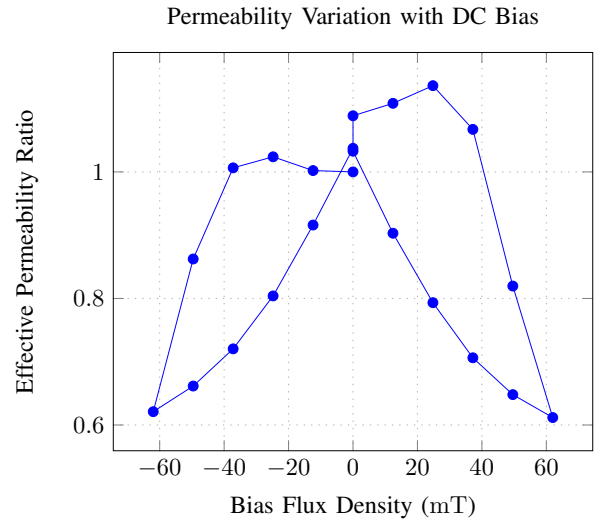


Fig. 17: Ratio of effective permeability  $\mu_{eff}$  (with bias) to initial permeability  $\mu_{r,i} = 125$  (without bias) of Fair-Rite 61 with ac flux swing held constant at 2.9 mT and dc bias slowly changing. The measurement was done on an ungapped toroid driven at a frequency of 10 MHz. The inductance of the device under test is inferred from the resonant frequency, which changes with dc bias, and the permeability ratio is equal to the inductance ratio.

## REFERENCES

- [1] D. V. Harburg, X. Yu, F. Herrault, C. G. Levey, M. G. Allen, and C. R. Sullivan, "Micro-fabricated thin-film inductors for on-chip power conversion," in *7th International Conference on Integrated Power Electronics Systems (CIPS)*. IEEE, 2013, pp. 6–8.
- [2] D. J. Perreault, J. Hu, J. M. Rivas, Y. Han, O. Leitermann, R. C. N. Pilawa-Podgurski, A. Sagneri, and C. R. Sullivan, "Opportunities and challenges in very high frequency power conversion," in *Twenty-Fourth Annual IEEE Applied Power Electronics Conference and Exposition (APEC)*, Feb 2009, pp. 1–14.
- [3] M. Araghchini, J. Chen, V. Doan-Nguyen, D. Harburg, D. Jin, J. Kim, M. S. Kim, S. Lim, B. Lu, D. Piedra, J. Qiu, J. Ranson, M. Sun, X. Yu, H. Yun, M. Allen, J. del Alamo, G. DesGroseilliers, F. Herrault, J. H. Lang, C. Levey, C. Murray, D. Otten, T. Palacios, D. J. Perreault, and C. R. Sullivan, "A technology overview of the powerchip development program," *IEEE Transactions on Power Electronics*, vol. 28, no. 9, pp. 4182–4201, 2013.
- [4] D. Giuliano, M. D'Asaro, J. Zwart, and D. Perreault, "Miniaturized low-voltage power converters with fast dynamic response," *Emerging and Selected Topics in Power Electronics, IEEE Journal of*, vol. 2, no. 3, pp. 395–405, Sept 2014.
- [5] C. O. Mathuna, N. Wang, S. Kulkarni, R. Anthony, C. N. J. Oliver, P. Alou, V. Svikovic, J. A. Cobos, J. Cortes, F. Neveu, C. Martin, B. Allard, F. Voiron, B. Knott, C. Sandner, G. Maderbacher, J. Pichler, M. Agostinelli, A. Anca, and M. Breig, "Power supply with integrated passives - the eu fp7 powerswipe project," in *8th International Conference on Integrated Power Electronics Systems (CIPS)*. IEEE, 2014, pp. 25–27.

- [6] R. C. N. Pilawa-Podgurski, A. D. Sagneri, J. M. Rivas, D. I. Anderson, and D. J. Perreault, "Very high frequency resonant boost converters," in *Power Electronics Specialists Conference, 2007. PESC 2007. IEEE*, June 2007, pp. 2718–2724.
- [7] J. Hu, A. D. Sagneri, J. M. Rivas, Y. Han, S. M. Davis, and D. J. Perreault, "High frequency resonant sepic converter with wide input and output voltage ranges," in *Power Electronics Specialists Conference, 2008. PESC 2008. IEEE*, June 2008, pp. 1397–1406.
- [8] P. Shamsi and B. Fahimi, "Design and development of very high frequency resonant dc-dc boost converters," *Power Electronics, IEEE Transactions on*, vol. 27, no. 8, pp. 3725–3733, Aug 2012.
- [9] M. Rodriguez, Y. Zhang, and D. Maksimovic, "High-frequency pwm buck converters using gan-on-sic hemts," *Power Electronics, IEEE Transactions on*, vol. 29, no. 5, pp. 2462–2473, May 2014.
- [10] W. Liang, J. Glaser, and J. Rivas, "13.56 mhz high density dc-dc converter with pcb inductors," *Power Electronics, IEEE Transactions on*, vol. 30, no. 8, pp. 4291–4301, Aug 2015.
- [11] Z. Zhang, j. lin, y. zhou, and X. Ren, "Analysis and decoupling design of a 30 mhz resonant sepic converter," *Power Electronics, IEEE Transactions on*, vol. PP, no. 99, pp. 1–1, 2015.
- [12] A. Knott, T. Andersen, P. Kamby, J. Pedersen, M. Madsen, M. Kovacevic, and M. Andersen, "Evolution of very high frequency power supplies," *Emerging and Selected Topics in Power Electronics, IEEE Journal of*, vol. 2, no. 3, pp. 386–394, Sept 2014.
- [13] M. Madsen, A. Knott, and M. Andersen, "Low power very high frequency switch-mode power supply with 50 v input and 5 v output," *Power Electronics, IEEE Transactions on*, vol. 29, no. 12, pp. 6569–6580, Dec 2014.
- [14] W. Cai, Z. Zhang, X. Ren, and Y.-F. Liu, "A 30-mhz isolated push-pull vhf resonant converter," in *Applied Power Electronics Conference and Exposition (APEC), 2014 Twenty-Ninth Annual IEEE*, March 2014, pp. 1456–1460.
- [15] S. Lim, D. M. Otten, and D. J. Perreault, "Power conversion architecture for grid interface at high switching frequency," in *Applied Power Electronics Conference and Exposition (APEC), 2014 Twenty-Ninth Annual IEEE*, March 2014, pp. 1838–1845.
- [16] A. J. Hanson, J. A. Belk, S. Lim, C. R. Sullivan, and D. J. Perreault, "Measurements and performance factor comparisons of magnetic materials at high frequency," in *IEEE Energy Conversion Congress and Exposition (ECCE)*. IEEE, 2015.
- [17] Y. Han, G. Cheung, A. Li, C. R. Sullivan, and D. J. Perreault, "Evaluation of magnetic materials for very high frequency applications," *IEEE Transactions on Power Electronics*, pp. 425–435, 2008.
- [18] S. A. Mulder, "Fit formulae for power loss in ferrites and their use in transformer design," in *Proceedings of the International Power Conversion Conference*, 1993, pp. 345–345.
- [19] S. A. Mulder, "Loss formulas for power ferrites and their use in transformer design," *Philips Components*, p. 16, 1994, also in PCIM 1995.
- [20] T. G. W. Stijntjes, "Power ferrites: Performance and microstructure," in *ICF5*, no. C1-01, 1989, p. 587.
- [21] L. M. Bosley, "Data sheets provide clues for optimizing selection of smps ferrite core material," in *PCIM*, vol. 19, 1993, pp. 13–13.
- [22] A. Goldman, *Modern ferrite technology*. Springer, 2006.
- [23] F. Alves, R. Lebourgeois, and T. Waeckerle, "Soft magnetic materials for electrical engineering: State of the art and recent advances," *European transactions on electrical power*, vol. 15, no. 6, pp. 467–479, 2005.
- [24] "Soft ferrite cores: A user's guide," 2011. [Online]. Available: <http://www.transformer-assn.org/Soft\Ferrite\Cores\User\%20Guide.pdf>
- [25] F. Forest, E. Laboure, T. Meynard, and M. Arab, "Analytic design method based on homothetic shape of magnetic cores for high-frequency transformers," *Power Electronics, IEEE Transactions on*, vol. 22, no. 5, pp. 2070–2080, 2007.
- [26] T. M. Undeland, J. Lode, R. Nilssen, W. P. Robbins, and N. Mohan, "A single-pass design method for high-frequency inductors," *Industry Applications Magazine, IEEE*, vol. 2, no. 5, pp. 44–51, 1996.
- [27] M. Bogs and W. Holubarsch, "Design principles for high frequency power transformer materials," *Le Journal de Physique IV*, vol. 7, no. C1, pp. C1–117, 1997.
- [28] "Soft ferrites and accessories data handbook," Ferroxcube International Holding B.V., Tech. Rep., 2013.
- [29] M. S. Rylko, B. J. Lyons, J. G. Hayes, and M. G. Egan, "Revised magnetics performance factors and experimental comparison of high-flux materials for high-current dc-dc inductors," *Power Electronics, IEEE Transactions on*, vol. 26, no. 8, pp. 2112–2126, 2011.
- [30] D. Yao and C. R. Sullivan, "Effect of capacitance on eddy-current loss in multi-layer magnetic films for mhz magnetic components," in *IEEE Energy Conversion Congress and Exposition (ECCE)*. IEEE, 2009, pp. 1025–1031.
- [31] M. E. Dale and C. R. Sullivan, "Comparison of power loss in single-layer and multi-layer windings with physical constraints or strong harmonics," in *IEEE International Symposium on Industrial Electronics*, 2006, pp. 1467–1473.
- [32] W. G. Hurley, E. Gath, and J. G. Breslin, "Optimizing the ac resistance of multilayer transformer windings with arbitrary current waveforms," *IEEE Transactions on Power Electronics*, vol. 15, no. 2, pp. 369–376, Mar 2000.
- [33] C. R. Sullivan, "Layered foil as an alternative to litz wire: Multiple methods for equal current sharing among layers," in *IEEE 15th Workshop on Control and Modeling for Power Electronics (COMPEL)*, June 2014, pp. 1–7.
- [34] S. Lim, D. M. Otten, and D. J. Perreault, "Ac-dc power factor correction architecture suitable for high frequency operation," *IEEE Transactions on Power Electronics*, IEEE Early Access.
- [35] E. C. Snelling, *Soft Ferrites, Properties and Applications*, 2nd ed. Butterworths, 1988.
- [36] C. R. Sullivan, "Optimal choice for number of strands in a litz-wire transformer winding," *Power Electronics, IEEE Transactions on*, vol. 14, no. 2, pp. 283–291, Mar 1999.
- [37] C. R. Sullivan and R. Y. Zhang, "Simplified design method for litz wire," in *IEEE Applied Power Electronics Conference and Exposition (APEC)*. IEEE, 2014, pp. 2667–2674.
- [38] C. P. Steinmetz, "On the law of hysteresis," *American Institute of Electrical Engineers, Transactions of the*, vol. IX, no. 1, pp. 1–64, Jan 1892.
- [39] Nizn materials. Ceramic Magnetics, Inc. [Online]. Available: <http://www.cmi-ferrite.com/Materials/NiZn.htm>
- [40] Material data sheets. Fair-Rite Products Corp. [Online]. Available: <http://www.fair-rite.com/newfair/materials.htm>
- [41] Power electronics cores. Metmagnetics. [Online]. Available: <http://www.mtmgx.com/products-overview/cores/>
- [42] General material properties. Micrometals, Inc. [Online]. Available: [http://www.micrometals.com/materials\\_index.html](http://www.micrometals.com/materials_index.html)
- [43] Ferrite: Nizn. National Magnetics Group. [Online]. Available: [http://www.magneticsgroup.com/m\\_ferr\\_nizn.htm](http://www.magneticsgroup.com/m_ferr_nizn.htm)
- [44] J. Muhlethaler, J. Biela, J. Kolar, and A. Ecklebe, "Core losses under the dc bias condition based on steinmetz parameters," *Power Electronics, IEEE Transactions on*, vol. 27, no. 2, pp. 953–963, Feb 2012.
- [45] H. Kosai, Z. Turgut, and J. Scofield, "Experimental investigation of dc-bias related core losses in a boost inductor," *Magnetics, IEEE Transactions on*, vol. 49, no. 7, pp. 4168–4171, July 2013.
- [46] G. Skutt and F. Lee, "Characterization of dimensional effects in ferrite-core magnetic devices," in *Power Electronics Specialists Conference, 1996. PESC '96 Record., 27th Annual IEEE*, vol. 2, Jun 1996, pp. 1435–1440 vol.2.
- [47] J. Reinert, A. Brockmeyer, and R. De Doncker, "Permeability enhancement by induced displacement current in magnetic material with high permittivity," *Journal of Magnetism and Magnetic Materials*, vol. 313, no. 1, pp. 47–51, Jan 2007.
- [48] A. van den Bossche and V. Valchev, *Inductors and Transformers for Power Electronics*. Taylor and Francis Group, 2005.
- [49] Magnetics design handbook section 4 - power transformer design. Texas Instruments. [Online]. Available: [www.ti.com/lit/ml/slup126/slup126.pdf](http://www.ti.com/lit/ml/slup126/slup126.pdf)
- [50] IEEE, "Ieee standard for test procedures for magnetic cores, standard 393-1991," Tech. Rep., 1992.
- [51] IEC, "Cores made of soft magnetic materials-measuring methods, international standard 62044-1," Tech. Rep., 2002-2005.
- [52] A. Goldberg, "Development of magnetic components for 1-10 mhz dc/dc converters," Ph.D. dissertation, Massachusetts Institute of Technology, 1988.
- [53] C. Xiao, G. Chen, and W. G. H. Odendaal, "Overview of power loss measurement techniques in power electronics systems," *IEEE Transactions on Industry Applications*, vol. 43, no. 3, pp. 657–664, 2007.
- [54] D. Christen, U. Badstuebner, J. Biela, and J. W. Kolar, "Calorimetric power loss measurement for highly efficient converters," in *2010 International Power Electronics Conference (IPEC)*. IEEE, 2010, pp. 1438–1445.
- [55] J. M. Miller, C. W. Ayers, L. E. Seiber, and D. B. Smith, "Calorimetric evaluation of inverter grade metalized film capacitor est," in *IEEE Energy Conversion Congress and Exposition (ECCE)*, Sept 2012, pp. 2157–2163.

- [56] R. Linkous, A. W. Kelley, and K. C. Armstrong, "An improved calorimeter for measuring the core loss of magnetic materials," in *Applied Power Electronics Conference and Exposition, 2000. APEC 2000. Fifteenth Annual IEEE*, vol. 2. IEEE, 2000, pp. 633–639.
- [57] V. J. Thottuvelil, T. G. Wilson, and H. A. Owen Jr, "High-frequency measurement techniques for magnetic cores," *IEEE Transactions on Power Electronics*, vol. 5, no. 1, pp. 41–53, 1990.
- [58] T. Sato and Y. Sakaki, "100 kHz–10 MHz iron loss measuring system," *IEEE Transactions on Magnetics*, vol. 23, no. 5, pp. 2593–2595, 1987.
- [59] M. Mu, Q. Li, D. Gilham, F. C. Lee, and K. D. T. Ngo, "New core loss measurement method for high frequency magnetic materials," in *IEEE Energy Conversion Congress and Exposition (ECCE)*. IEEE, 2010, pp. 4384–4389.
- [60] M. Mu, F. C. Lee, Q. Li, D. Gilham, and K. D. T. Ngo, "A high frequency core loss measurement method for arbitrary excitations," in *IEEE Applied Power Electronics Conference and Exposition (APEC)*. IEEE, 2011, pp. 157–162.
- [61] D. Hou, M. Mu, F. Lee, Q. Li *et al.*, "New core loss measurement method with partial cancellation concept," in *IEEE Applied Power Electronics Conference and Exposition (APEC)*. IEEE, 2014, pp. 746–751.
- [62] C. F. Foo and D. M. Zhang, "A resonant method to construct core loss of magnetic materials using impedance analyser," in *IEEE Power Electronics Specialists Conference (PESC)*, vol. 2. IEEE, 1998, pp. 1997–2002.
- [63] J. Reinert, A. Brockmeyer, and R. De Doncker, "Calculation of losses in ferro- and ferrimagnetic materials based on the modified steinmetz equation," *Industry Applications, IEEE Transactions on*, vol. 37, no. 4, pp. 1055–1061, Jul 2001.
- [64] J. Li, T. Abdallah, and C. R. Sullivan, "Improved calculation of core loss with nonsinusoidal waveforms," in *Industry Applications Conference, 2001. Thirty-Sixth IAS Annual Meeting. Conference Record of the 2001 IEEE*, vol. 4, Sept 2001, pp. 2203–2210 vol.4.
- [65] K. Venkatachalam, C. R. Sullivan, T. Abdallah, and H. Tacca, "Accurate prediction of ferrite core loss with nonsinusoidal waveforms using only steinmetz parameters," in *Computers in Power Electronics, 2002. Proceedings. 2002 IEEE Workshop on*, June 2002, pp. 36–41.
- [66] J. Muhlethaler, J. Biela, J. Kolar, and A. Ecklebe, "Improved core-loss calculation for magnetic components employed in power electronic systems," *Power Electronics, IEEE Transactions on*, vol. 27, no. 2, Feb 2012.
- [67] T. Lee, *Planar Microwave Engineering: A Practical Guide to Theory, Measurement, and Circuits*. Cambridge University Press, 2004.



**Alex J. Hanson** (S'15) received the B.E. degree in electrical engineering with highest honors from the Thayer School of Engineering at Dartmouth College, Hanover, NH in 2014, where he worked to develop on-chip thin-film power magnetic components. He is currently working toward the Ph.D. degree at the Massachusetts Institute of Technology, Cambridge, MA. His research interests include both component- and system-level power electronics to enable new applications and improve performance in existing spaces.



**Julia A. Belk** (S'15) was born in Boston, MA, on September 27, 1995. She is currently pursuing the B.S. degree in electrical engineering from the Massachusetts Institute of Technology, Cambridge, MA.

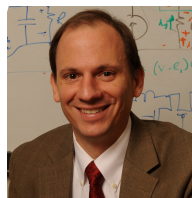


**Seungbum Lim** (S'10) received the B.S. degree in electrical engineering from Seoul National University, Seoul, Korea, in 2010 and the S.M. degree in electrical engineering from the Massachusetts Institute of Technology, Cambridge, in 2012, where he is currently working toward the Ph.D. degree in the Laboratory of Electromagnetic and Electronic Systems. His research interests include power electronics, resonant converters, soft-switching techniques, and RF power amplifiers.



**Charles R. Sullivan** (S'93–M'96–SM'12–F'14) received the B.S. degree in electrical engineering (with highest honors) from Princeton University, Princeton, NJ, in 1987 and the Ph.D. degree in electrical engineering from the University of California, Berkeley, in 1996. He is presently a Professor of Engineering at the Thayer School of Engineering at Dartmouth, Hanover, NH. His research includes work on design optimization of magnetics and other passive components for high-frequency power conversion, thin-film magnetic materials and devices for power applications, and applications of power electronics including energy efficiency and renewable energy.

Dr. Sullivan received the National Science Foundation CAREER Award and two Power Electronics Society Prize Paper Awards.



**David J. Perreault** (S'91–M'97–SM'06–F'13) received the B.S. degree from Boston University, Boston, MA, and the S.M. and Ph.D. degrees from the Massachusetts Institute of Technology, Cambridge, MA. In 1997 he joined the MIT Laboratory for Electromagnetic and Electronic Systems as a Postdoctoral Associate, and became a Research Scientist in the laboratory in 1999. In 2001, he joined the MIT Department of Electrical Engineering and Computer Science, where he is presently Professor and Associate Department Head. His research

interests include design, manufacturing, and control techniques for power electronic systems and components, and in their use in a wide range of applications. He also consults in industry, and is co-founder of Eta Devices, a startup company focusing on high-efficiency RF power amplifiers.

Dr. Perreault received the Richard M. Bass Outstanding Young Power Electronics Engineer Award, the R. David Middlebrook Achievement Award, the ONR Young Investigator Award, and the SAE Ralph R. Teetor Educational Award, and is co-author of seven IEEE prize papers.